

Candidate members of the Pal 5, GD-1, Cetus Polar, and Orphan tidal stellar halo streams from SDSS DR9, LAMOST DR3 and APOGEE catalogues

Guang-Wei Li¹, Brian Yanny², Hao-Tong Zhang¹, Zong-rui Bai¹, Yue Wu¹, Yi-qiao Dong¹,
Ya-juan Lei¹, Hai-long Yuan¹, Yong-Hui Hou³, Yue-Fei Wang³ and Yong Zhang³

¹ Key Lab for Optical Astronomy, National Astronomical Observatories, Chinese Academy of Sciences,
Beijing 100012, China; *lgw@bao.ac.cn*

² Fermi National Accelerator Laboratory, Batavia, IL 60510, USA

³ Nanjing Institute of Astronomical Optics & Technology, National Astronomical Observatories, Chinese
Academy of Sciences, Nanjing 210042, China

Abstract We present candidate members of the Pal 5, GD-1, Cetus Polar, and Orphan tidal stellar streams found in LAMOST DR3, SDSS DR9 and APOGEE catalogs. In LAMOST DR3, we find 20, 4, 24 high confidence candidates of tidal streams GD-1, Cetus Polar and Orphan respectively. We also list from the SDSS DR9 spectroscopic catalog 59, 118, 10 high confidence candidates of tidal streams Cetus Polar, Orphan and Pal 5, respectively. Furthermore, we find 7 high confidence candidates of the Pal 5 tidal stream in APOGEE data. Compared with SDSS, the new candidates from LAMOST DR3 are brighter, so that together, more of the color-magnitude diagram, including the giant branch can be explored. Analysis of SDSS data shows that there are 3 metallicity peaks of the Orphan stream and also shows some spatial separation. LAMOST data confirms multiple metallicities in this stream. The metallicity, given by the higher resolution APOGEE instrument, of the Pal 5 tidal stream is $[\text{Fe}/\text{H}] \sim -1.2$, higher than that given earlier by SDSS spectra. Many previously unidentified stream members are tabulated here for the first time, along with existing members, allowing future researchers to further constrain the orbits of these objects as they move within the Galaxy's dark matter potential.

Key words: Galaxy: structure general: stream – Galaxy: structure individual (GD-1, Orphan, Cetus, Pal 5)

1 INTRODUCTION

There are two popular models for the how our Galaxy formed. The first, given by Eggen et al. (1962), sug-

(1978) suggested that an inner halo may have come from a large early collapse, but the outer halo independently evolved over a much longer period of time, and during this time, many small stellar systems merged into the halo, and were tidally disrupted by the Galaxy's potential. The standard Λ CDM cosmological model also favors big galaxies growing from the merger of smaller units.

The largest and most famous Milky Way halo stellar stream is that associated with the Sagittarius dwarf galaxy (Ibata et al., 1994), mapped out in 2MASS giants by Majewski et al. (2003). Much progress in stream detection occurred with the release of the SDSS dataset (York et al., 2000). Four streams: GD-1, Orphan, Cetus Polar Stream (CPS), and the Pal 5 tidal stream were discovered using SDSS data. GD-1 is a 63° narrow stream, found by Grillmair & Dionatos (2006). Later, Willett et al. (2009) fit an orbit. Yanny et al. (2009a) noticed that there is a tidal stream near the Sgr trailing tidal tail which was named the CPS by Newberg et al. (2009). Its parameters were given by Yam et al. (2013) using SDSS DR8. The Orphan stream was found by Grillmair & Dionatos (2006) and Belokurov et al. (2006), but its orbital parameters were not clear until Newberg et al. (2010) gave them using SDSS DR 7. Pal 5 is a globular cluster which is being disrupted. Its long tail was firstly discovered by Odenkirchen et al. (2001), which spans more than 23° (Carlberg et al., 2012), and is the most obvious stream associated with a Galactic globular cluster.

Having an accurate census of stream members, as well as their spectroscopic properties (including radial velocity, and parameters which may be used to estimate absolute magnitude – and thus distance) is crucial to determining accurate orbits of the streams. In turn, having an accurate orbit for a set of streams allows us to probe the (dark matter dominated) gravitational potential at a variety of distances and directions throughout the Milky Way's halo (Newberg et al., 2010).

A major unresolved question in Galactic dynamics is understanding in detail the shape (i.e. oblate, prolate, spherical, lumpy, changing-with-radius?) and extent (total mass and drop-off with radius) of our Galaxy's dark matter potential and the dark halo's shape and size. For instance, is the halo triaxial in nature as suggested by Law, Majewski and Johnston (2009)? Having extensive, accurate stellar stream membership information, along with radial velocity and photometric parallax information for member stars can help resolve this important question. This work adds to our list of known stream members, with spectroscopic velocity and other stellar parameters for four halo streams.

The Large Sky Area Multi-Object Fiber Spectroscopic Telescope (LAMOST, also called the Guo Shou Jing Telescope) (Cui et al., 2012; Wang et al., 1996; Su & Cui, 2004) is a special reflecting Schmidt telescope with field of view (FOV) 5° and effective aperture 3.6m - 4.9 m. There are 4,000 fibers on its focal plane and they can record 4,000 spectra at once. Its wavelength coverage is 365 nm - 900 nm with $R \sim 1,800$. Each of 16 spectrographs records images of 250 fibers on a $4136 \text{ pixel} \times 4160 \text{ pixel}$ CCD. As of May 30, 2015, more than 3 million A, F, G and K stellar spectra with parameters have been released (Luo et al., 2012; Zhao et al., 2012)(see <http://dr3.lamost.org/>).

In this paper, we search for and describe parameters for high confidence stellar candidates of the GD-1, Orphan, CPS and Pal 5 tidal stream in the spectral data of LAMOST DR3, SDSS DR9 (Yanny et al., 2009b)

2 CANDIDATES OF STREAMS

We search for stream members, primarily giants ($0 < \log g < 3.5$), in the LAMOST DR3, SDSS DR9 APOGEE spectral databases. As is common in the literature, magnitudes with subscript 0 indicate they have been corrected by the extinction given by Schlegel et al. (1998), (not the more recent Schlafly & Finkbeiner (2011) – the differences are tiny at these higher Galactic $|b|$). All g and r band magnitudes in this paper are from SDSS DR9. Because the $[\text{Fe}/\text{H}]$ values estimated by the standard LAMOST processing pipeline (Wu et al., 2014) have a lower limit of -2.4 , there is no star with quoted $[\text{Fe}/\text{H}]$ less than -2.4 in LAMOST DR3. For SDSS stars with spectra, Newberg et al. (2009) found the quoted FEHWBG (Wilhelm et al., 1999) (WBG) parameter is a better measure of metallicity than FEHADOP for blue BHBs, so we use WBG metallicity for stars with $(g - r)_0 < 0.2$ and FEHADOP (adopted) metallicity for stars with $(g - r)_0 > 0.2$. For a star observed many times, we only retain the spectrum with the highest Signal-to-noise ratio (SNR) in the g and r bands for LAMOST spectra, and that with the highest SNR for SDSS and APOGEE. We convert radial velocities to the Galactic standard of rest velocities (V_{gsr}) using the formula $V_{gsr} = RV + 10.1 \cos b \cos l + 224 \cos b \sin l + 6.7 \sin b$, where RV is the heliocentric radial velocity in km s^{-1} , while (l, b) are the Galactic coordinates of the star.

For each of the four streams accessible with LAMOST or SDSS or APOGEE spectroscopy, and which have SDSS g & r -band photometry, we search in the up to seven-dimensional space of: 1,2) (l, b) position along the orbit; 3) distance (determined by photometric parallax using the cataloged star’s color, magnitude and spectral type (giant or dwarf) depending on surface gravity); 5) velocity and (lack of measureable) 6,7) proper motion to select candidates and give confidence estimates of candidates’ membership in a given stream. We give each candidate a number (1, 2 or 3) to describe our confidence in stream membership, with a higher number indicating lower confidence.

2.1 Candidates of the GD-1 Stream

The study of Willett et al. (2009) has given all the GD-1 stream candidates present in SDSS data, so here we only search for GD-1 candidates in LAMOST DR3, using the same method as Willett et al. (2009). All giant candidates match the following criteria:

1) The GD-1 positional locus is $\delta = -864.5161 + 13.22518\alpha - 0.06325544\alpha^2 + 0.0001009792\alpha^3$. Candidates should be within $\delta \pm 1^\circ$.

2) There are 7 set (regions) of stars close in position and velocity listed in Willett et al. (2009). Regions 1, 4, 5, 6 have high confidence stream members. Between Region 1 and Region 4, Region 2 is more reliable than Region 3 (in terms of groupings of velocities and color-magnitude properties of candidate stars), so we only use data of Region 2. Beyond Region 6, the only data we can use is Region 7 though it is not so reliable as Region 1, 4, 5, 6. Thus, we use V_{gsr} in Region 1, 2, 4, 5, 6, 7 to select candidates. We generate the velocity trendline by interpolation and extrapolation of velocities of these regions, then select candidates within 30 km s^{-1} around the trendline.

3) Galactic proper motions and errors are calculated from equatorial proper motions with errors in the SDSS DR9 (based on the UCAC4 catalog). We select high confidence candidates by limiting their proper

4) Metallicities $[\text{Fe}/\text{H}]$ should be in the range $[-2.5, -1.5]$.

Fig. 1 shows their metallicity distribution. As shown by Fig. 2 in Gao et al. (2015), LAMOST overestimates metallicities for the most metal-poor stars, and their variance is larger than metal-rich stars. The metallicity distribution of GD-1 member candidates from SDSS DR7, shown in Fig. 5 in Willett et al. (2009), is also broad. Thus, although these stars span broad metallicity range, we still consider them candidate members of the GD-1 stream.

The red polygon in Fig. 2 shows the area where the high confidence candidates rest. Their color-magnitude diagram (CMD, hereafter) is shown in Fig. 3. We estimate their absolute magnitudes as they are giants similar to metal poor giants in the globular cluster M92, using the M92 isochrone and then remove candidate stars with implied distances far from the GD-1 stream distance. This leaves us with 20 high confidence candidates. Magnitudes of the brightest five stars, which we believe are GD-1 members, are not reliable because SDSS CCD saturates around $r \sim 14.5$. For a stream, brighter members are fewer, so if these five bright stars really belong to GD-1 stream, they will greatly help us to understand the stream.

One star in Region 1 has no SDSS photometry, but we still retain it, because there are only two candidates in Region 1, if it is really a GD-1 member, it would be valuable to study this Region.

The confidence level of each candidate is given based on its position on Fig. 2 and Fig. 3. Let Dv_i denote the difference between $V_{g_{sr}}$ of the i th candidate and the trendline at its longitude, and $\sigma_1^2 = \sum_{i \in \phi} Dv_i^2 / (n - 1)$, where $\phi = \{i | |Dv_i| < 3\sigma_1\}$ and n is the number of the elements in ϕ ; Let Dc_i denote the difference between $(g - r)_0$ of the i th candidate and the M92 isochrone at its g_{corr} , and $\sigma_2^2 = \sum_{i \in \psi} Dc_i^2 / (m - 1)$, where $\psi = \{i | |Dc_i| < 3\sigma_2\}$ and m is the number of the elements in ϕ . Then we calculate the f_i for the i th candidate by the formula: $f_i = (\frac{Dv_i}{\sigma_1})^2 + (\frac{Dc_i}{\sigma_2})^2$. If $f_i \leq 2$, then the confidence level of the i th candidate is set to be 1; if $2 < f_i \leq 10$, then the confidence level is set to be 2; if $f_i > 10$, then the confidence level is set to be 3.

We searched for GD-1 candidates in APOGEE spectral data, but found none.

2.2 Candidates of the Cetus Polar Stream

We select CPS candidates by the method given by Yam et al. (2013). All giant candidates should match the following criteria:

- 1) Metallicities should be in $[-2.5, -1.5]$;
- 2) Distances to the Galactic great circle $l = 143^\circ$ should be less than 15° ;
- 3) We find that the stream velocity formula $V_{g_{sr}} = -41.67 - (0.84 \times b) - (0.014 \times b^2)$ given by Yam et al. (2013) has a typographical error, and the correct formula is $V_{g_{sr}} = -41.67 + (0.84 \times b) + (0.014 \times b^2)$, and we use this. We select candidates within $V_{g_{sr}} \pm 20 \text{ km s}^{-1}$.

4) We use the fiducial sequence of NGC 5466 as a reference to select confidence candidates in the CMD, then use equation 2 in Yam et al. (2013) to calculate their corrected magnitudes g_{corr} . All stars should be within $-0.01800g_{corr}^3 + 0.98473g_{corr}^2 - 18.05165g_{corr} + 111.43819 - 0.04 < (g - r)_0 < -0.01800g_{corr}^3 + 0.98473g_{corr}^2 - 18.05165g_{corr} + 111.43819 + 0.04$ and $16 < g_{corr} < 18.5$.

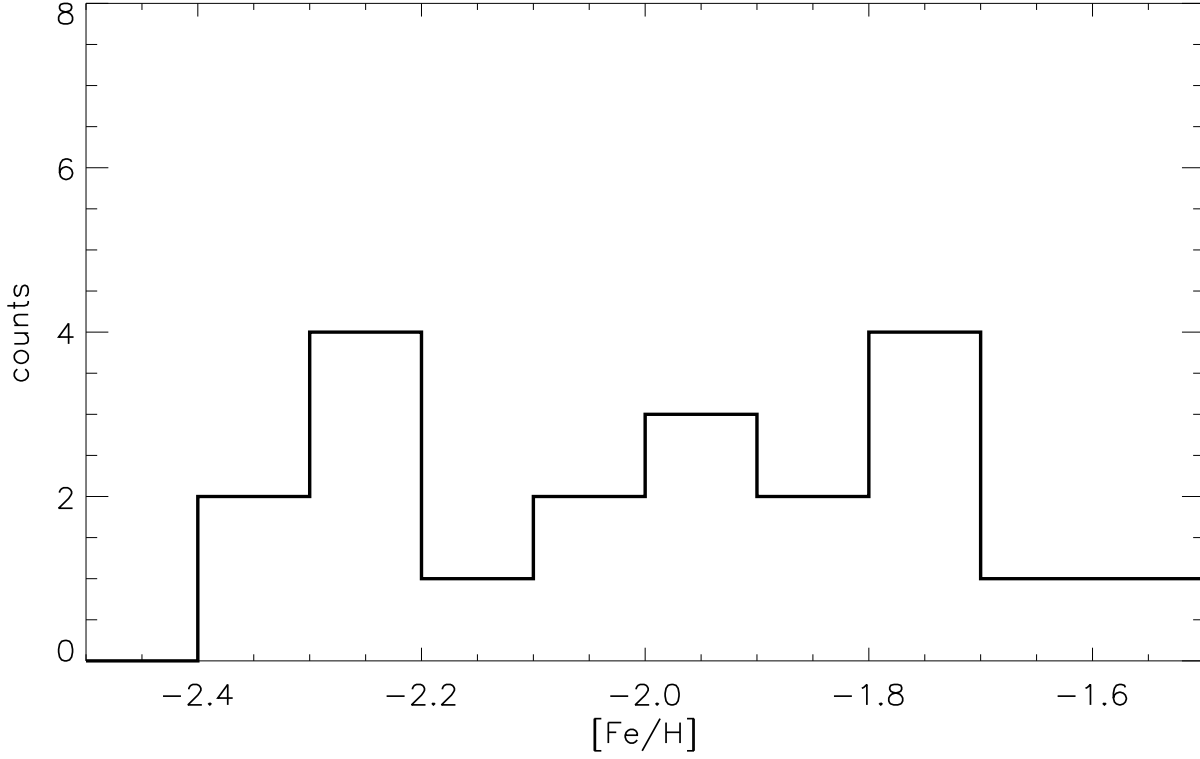


Fig. 1 The metallicity distribution of GD-1 stars in LAMOST DR3 that match all criteria.

Fig. 4 shows the CMD of these candidates in LAMOST DR3. The red circles are candidates we select. The stars denoted by crosses are candidates match criteria 1, 2, 3, 5. From Fig. 5 we can see that the colors of brighter Orphan stars go little upward from the fiducial sequence of NGC 5466, so we retain the top right corner star.

Additionally, we search for additional CPS candidates within SDSS DR9 by the same criteria as the above except the metallicity is restricted to $[-2.5, -2]$. Here obtain 59 candidates, including 21 BHBs. Fig. 5 shows the CMD of stars in CPS area. The red diamonds in the area enclosed by red and blue lines are the high confidence candidates. While many of these objects were already shown in Yam et al. (2013), there is, at red colors, a blue rectangle containing new candidates not searched in Yam et al. (2013). Fig. 6 shows the distribution range in Galactic coordinates. The central line is $l = 143^\circ$, the two dotted lines are the bounds 10° from the central line on the celestial sphere, and the crosses are the candidates in SDSS DR9. From this figure we can see that the width of CPS spans $\sim 20^\circ$, and almost all CPS candidates rest in $130^\circ < l < 160^\circ$ and $-25^\circ < b < -75^\circ$. CPS may extend beyond $l = 160^\circ$, this will need confirmation by another spectroscopic survey.

There is no APOGEE data available with corresponding photometric and proper motion data which overlaps CPS.

Because candidates of CPS from both SDSS DR9 and LAMOST DR3 are all within narrow strips in

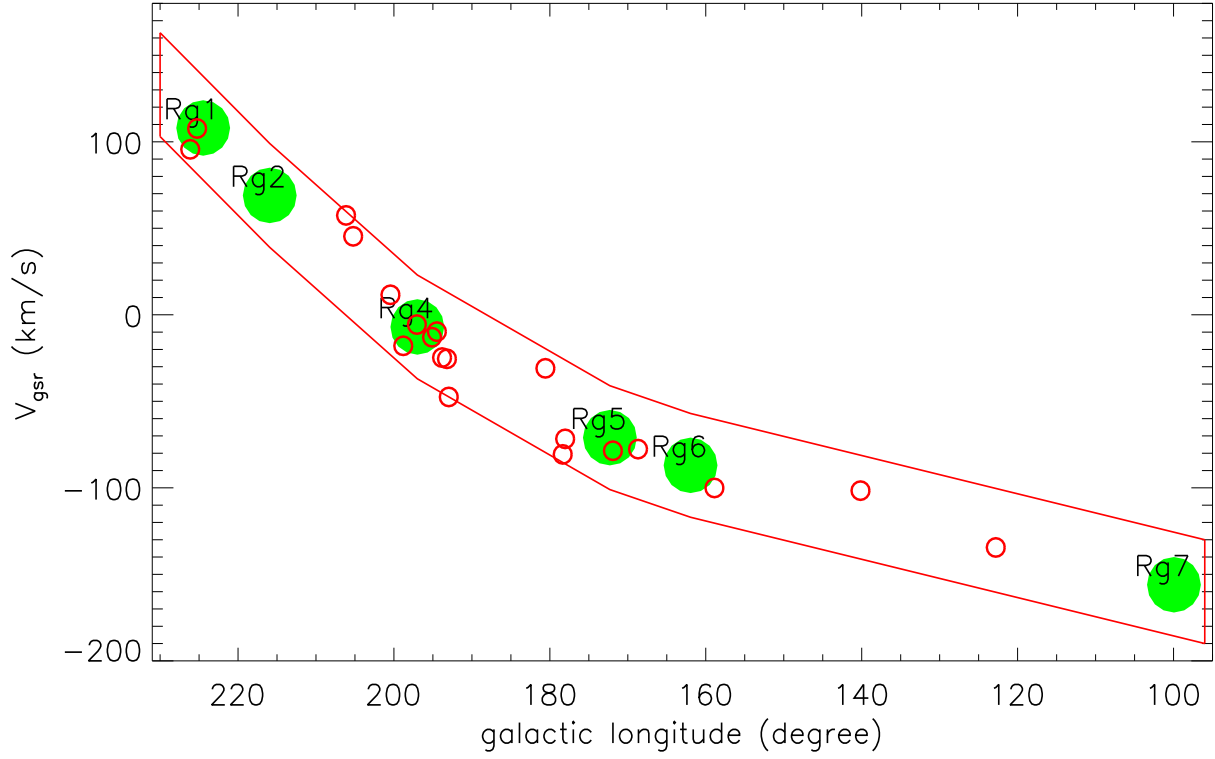


Fig. 2 Big green filled circles are V_{gsr} of regions given by Willett et al. (2009). The red polygon is the area where we select candidates of GD-1. The red circles are the high confidence candidates in LAMOST DR3.

2.3 Candidates of the Orphan Stream

We select the Orphan stream candidates by the method given by Newberg et al. (2010). In their paper, they defined a new coordinate system $(B_{Orphan}, \Lambda_{Orphan})$. Under this coordinate system, they defined a variable B_{corr} to let the stream locus be at $B_{corr} = 0$. Here, we also use these symbols with the same definitions. All giant candidates should match the following criteria:

- 1) Metallicities should be within $[-2.5, -1.6]$;
- 2) These candidates should be within $-2^\circ < B_{corr} < 2^\circ$.
- 3) We denote $T_{Orphan} = -0.0445\Lambda_{Orphan}^2 - 0.935\Lambda_{Orphan} + 130$. Then their Galactic standard of rest velocities V_{gsr} are within $T_{Orphan} \pm 35 \text{ km s}^{-1}$.
- 4) We calculate their g_{corr} by the formula: $g_{corr} = g_0 - 0.00022\Lambda_{Orphan}^2 + 0.034\Lambda_{Orphan}$.
- 5) Proper motions in R.A. and Dec. are all less than 6 mas/yr.
- 6) We shift the isochrone of M92 to the place where its BHBs are at $g_0 = 17.75$.

Fig. 7 shows the CMDs of Orphan stream candidates in SDSS and LAMOST data. The left panel and the right panel are the Orphan stream CMD of SDSS candidates and LAMOST candidates respectively. In each panel, the filled circles are stars in $T_{Orphan} \pm 17.5 \text{ km s}^{-1}$, while open circles are stars in $T_{Orphan} \pm 35 \text{ km s}^{-1}$. The isochrone of M92 is shifted to have its BHBs at $g_0 = 17.75$, as Newberg et al. (2010) did. In the LAMOST data, at least four star's photometry is unreliable.

In Fig. 8, the metallicity distributions of Orphan stream candidates in SDSS and LAMOST data are

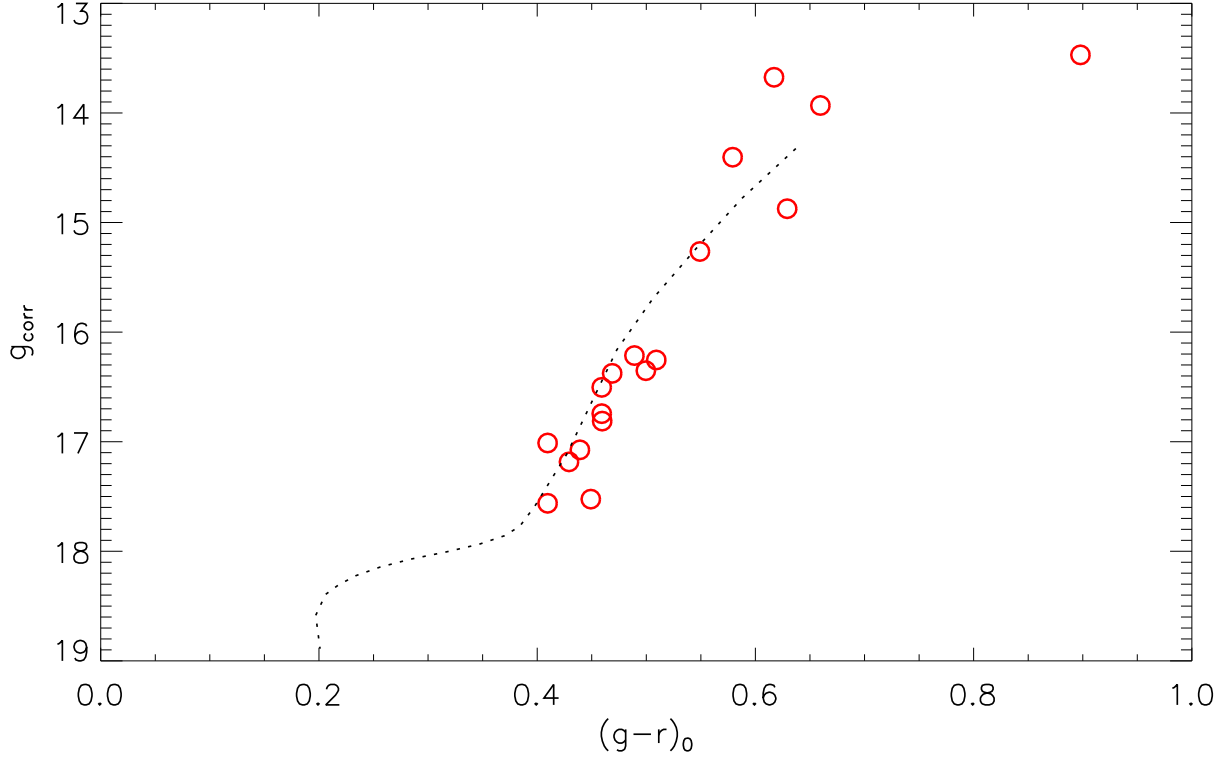


Fig.3 The red circles are the high confidence candidates of GD-1. The background line is the M92 fiducial locus. Each candidate is corrected to the distance of M92, which is 8.2kpc. Magnitudes of the top 5 stars are inaccurate due to saturation, and one star has no SDSS photometry – it is not shown in the figure.

bution of stars in $T_{Orphan} \pm 17.5 \text{ km s}^{-1}$, while the black histogram is that of stars in $T_{Orphan} \pm 35 \text{ km s}^{-1}$. We find that for SDSS candidates, there are 3 metallicity peaks which are $[-2.5, -2.3]$, $[-2.2, -1.9]$, and $[-1.9, -1.6]$. The last two peaks are confirmed by LAMOST data. Because LAMOST metallicity is cutoff by $[\text{Fe}/\text{H}] = -2.4$, the most metal-poor component does not appear in the LAMOST data. If three metallicity peaks are real, it suggests that there are 2-3 components in the Orphan stream or that other stellar populations from other objects are overlapping in space and velocity. Fig. 9 shows the V_{gsr} of SDSS candidates along the Λ_{Orphan} . The dash dot lines are $T_{Orphan} \pm 17.5 \text{ km s}^{-1}$, while the dash lines are $T_{Orphan} \pm 35 \text{ km s}^{-1}$. The stars with metallicity in $[-2.5, -2.3]$, $[-2.2, -1.9]$, and $[-1.9, -1.6]$ are marked by red, green and blue circles, respectively. From Fig. 9 we can see that compared to the stars with $[\text{Fe}/\text{H}]$ in $[-2.2, -1.9]$, $[-1.9, -1.6]$, almost all stars within the most metal-poor peak have $\Lambda_{Orphan} < 0$, with only 2 stars in $\Lambda_{Orphan} > 0$. This special metal pattern along the Λ_{Orphan} must relate to the origin and evolution histories of the stream, and need further study.

There is no APOGEE star candidate in the Orphan stream.

We use similar formulas in Sec. 2.1 to calculate confidence levels. Let Dv_i denote the difference between V_{gsr} of the i th candidate and the trendline $-0.0445\Lambda_{Orphan}^2 - 0.935\Lambda_{Orphan} + 130 \text{ km s}^{-1}$ at its Λ_{Orphan} , and $\sigma_1^2 = \sum_{i \in \phi} Dv_i^2 / (n - 1)$, where $\phi = \{i | |Dv_i| < 3\sigma_1\}$ and n is the number of the elements in ϕ ; Let Dc_i denote the difference between $(g-r)_0$ of the i th candidate and the M92 isochrone at its g_{corr} ,

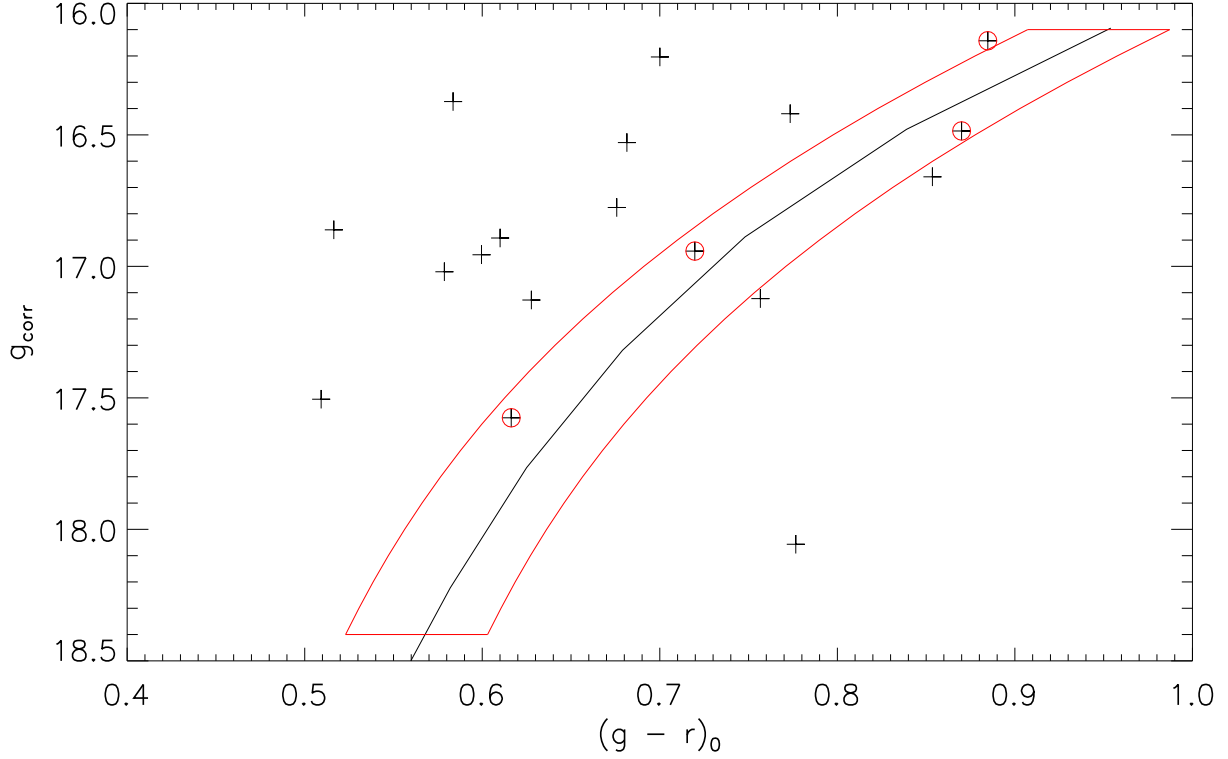


Fig.4 This figure shows the CPS candidates in LAMOST DR3. The stars denoted by crosses are stars which match criteria 1, 2, 3, 5, while the high confidence candidates are denoted by the red circles. The black line is the fiducial sequence of NGC 5466 shifted to the distance modulus 17.389. The area given by criteria 4 is shown by red lines.

Then we calculate the f_i for the i th candidate by the formula: $f_i = (\frac{Dv_i}{\sigma_1})^2 + (\frac{Dc_i}{\sigma_2})^2$. If $f_i \leq 2$, then the confidence level of the i th candidate is set to be 1; if $2 < f_i \leq 10$, then the confidence level is set to be 2; if $f_i > 10$, then the confidence level is set to be 3.

2.4 Pal 5 Tidal Stream

We select Pal 5 tidal stream candidates following the criteria from Kuzma et al. (2015). All giant candidates satisfy the following criteria:

1) Three positions $(226.3^\circ, -2.9^\circ)$, $(246^\circ, 7.9^\circ)$ and Pal 5 center $(229^\circ, -0.11^\circ)$ in (R.A., decl.) in Grillmair & Dionatos (2006) and the 11 centers of fields given in Table 1 by Kuzma et al. (2015) are used to calculate the trace of the Pal 5 tidal stream. Firstly, these positions are classified into 2 groups: the southern group consists of the cluster center and positions to the south; the northern group consists of the cluster center and positions to the north. Then these positions in each group are converted from (R.A., decl.) to (l, b) . For the trailing tail (northern part of the stream), we fit positions with a cubic polynomial, which is $b = 45.9816 - 0.0250988 * l - 0.0244554 * l^2 + 0.000332027 * l^3$. For the leading tail (southern part of the stream), we fit positions by a line, $b = 45.920122 - 0.010919619 * l$. All candidates should be within

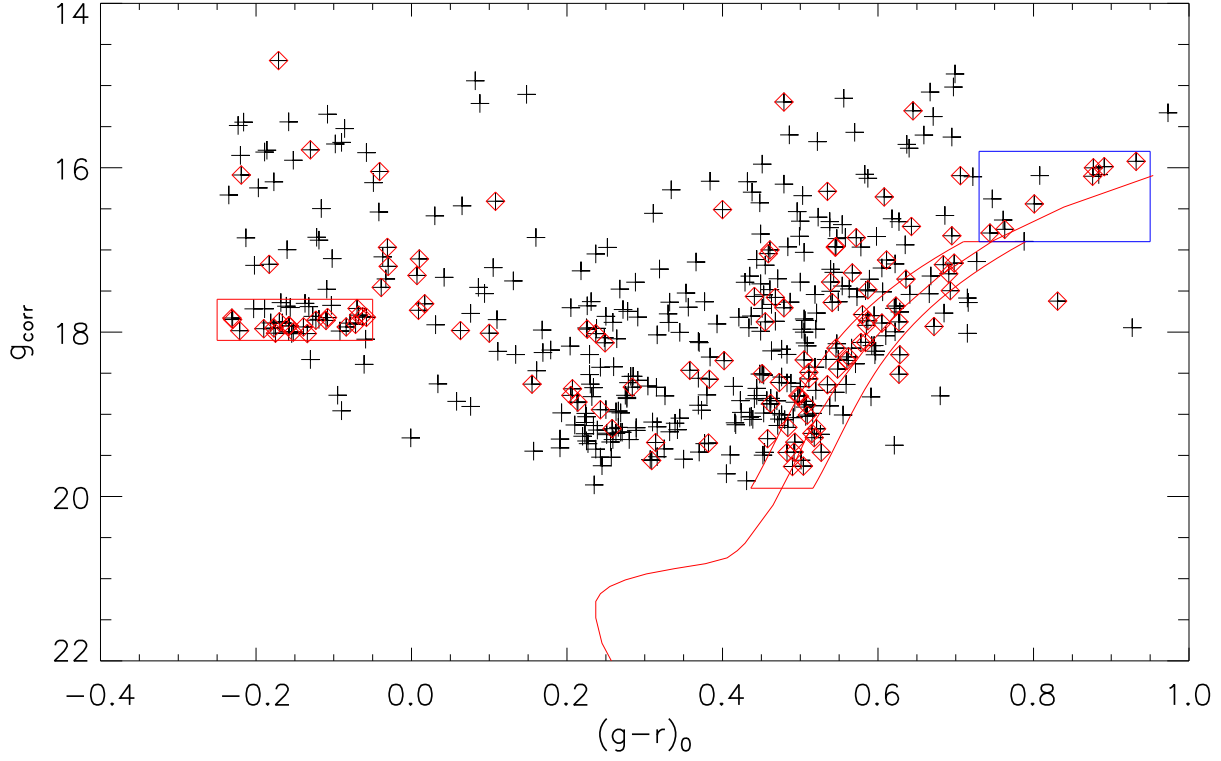


Fig. 5 The crosses are the candidates of the CPS in SDSS DR9 that match the criteria 2 - 5. The red diamonds are stars with metallicity in $[-2.5, -2.0]$. The area enclosed by red and blue lines is where we select candidates. The blue rectangle is the new area not given by Yam et al. (2013).

2) We use photometry of stars within $8.3'$ around Pal 5 the globular cluster center to generate a Pal 5 CMD.

3) Proper motions in R.A. and Dec. are all less than 6 mas/yr .

4) Metallicities are within $-2.5 < [\text{Fe}/\text{H}] < -0.6$. As RR Lyraes are variables, it is hard to get their real metallicity from one spectrum without knowing a phase. Thus, the metallicity criterion is extended to -2 . Secondly, there are very few (even no) candidates in these 3 catalogues on the Pal 5 long trailing tail, so every candidate is very valuable. We extend the metallicity criterion to -0.6 . In fact, only one member candidate (a red giant) has $[\text{Fe}/\text{H}] \sim -0.75$, while other red giant candidates have $[\text{Fe}/\text{H}]$ about within -1.4 ± 0.4 .

5) As mentioned by Kuzma et al. (2015), the velocity gradient along the trace is $1.0 \pm 0.1 \text{ km s}^{-1} \text{ deg}^{-1}$, so we use $RV_{\text{corr}} = RV - a$ to select candidates, where a is angular distance in degree to cluster center, $a < 0$ for leading tail stars, $a > 0$ for trailing tail stars, and RV is the line of sight velocity. RV_{corr} should be within $[-70, -45] \text{ km s}^{-1}$.

6) We use $0.00361996g_0^3 - 0.173359g_0^2 + 2.61828g_0 - 11.471$ to fit the fiducial sequence of Pal 5 red giant branch given by An et al. (2008), and use the criteria of $0.00361996g_0^3 - 0.173359g_0^2 + 2.61828g_0 - 11.471 + 0.1 < (g - r)_0 < 0.00361996g_0^3 - 0.173359g_0^2 + 2.61828g_0 - 11.471 - 0.15$, $16 < g_0 < 19.5$ and $-2 < [\text{Fe}/\text{H}] < -0.6$ to select candidates in red and asymptotic giant branch. In the horizontal branch

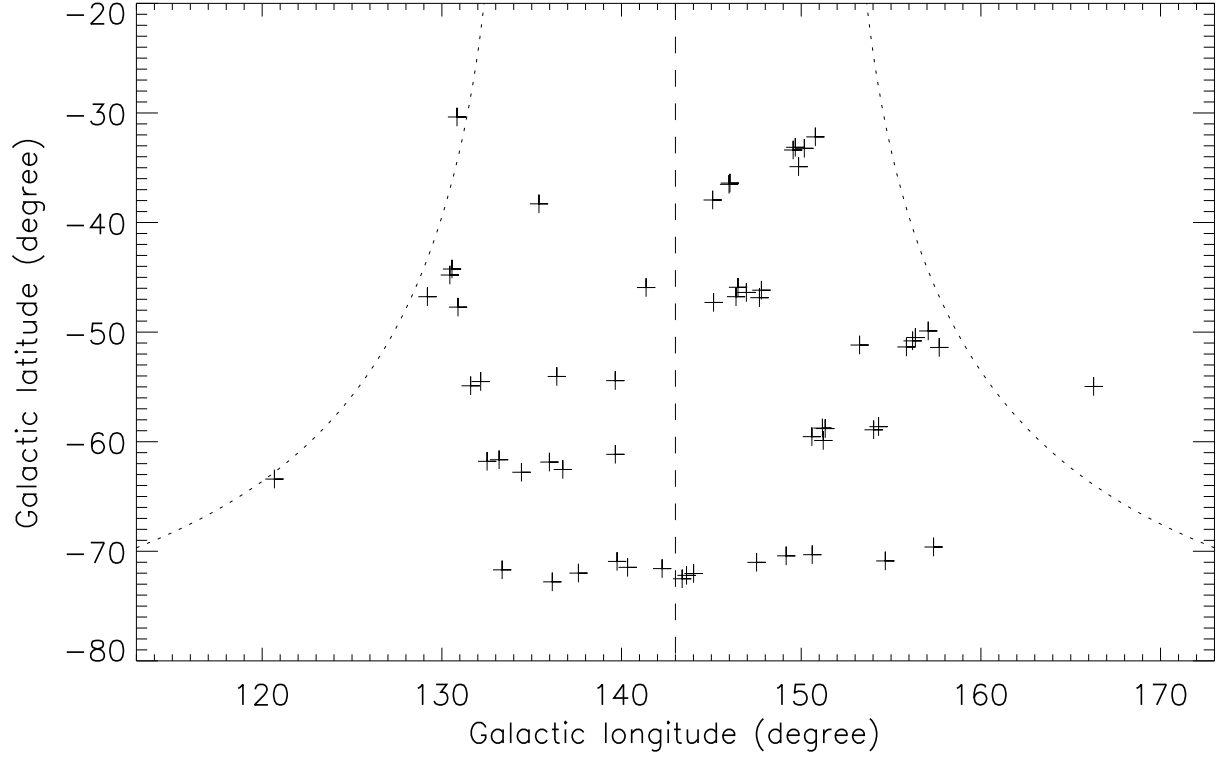


Fig. 6 This figure shows the distribution range of the CPS in Galactic coordinates. The central line is $l = 143^\circ$, the two dotted lines are the bounds 10° from the central line on the celestial sphere, while the crosses are the candidates in SDSS DR9.

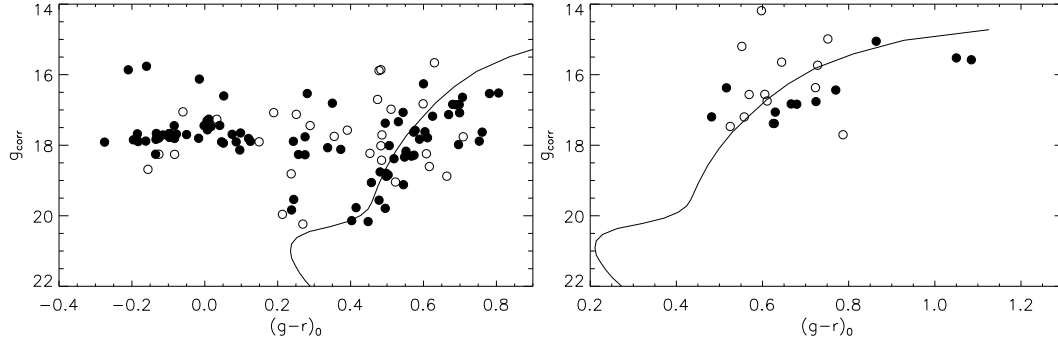


Fig. 7 The left panel and the right panel are the CMDs of Orphan stream candidates in SDSS and LAMOST data respectively. In each panel, the filled circles are stars within $T_{Orphan} \pm 17.5 \text{ km s}^{-1}$, while open circles are stars within $T_{Orphan} \pm 35 \text{ km s}^{-1}$. In each panel, the isochrone of M92 is shifted to have its BHBs at $g_0 = 17.75$.

We find no candidate in LAMOST data, but we find 8 red giants in APOGEE. We also find 5 RR Lyraes and 5 red giants in the SDSS DR9 spectra.

Fig. 10, 11, 12 and 13 are CMD, position, metallicity and line of sight velocity distributions of Pal 5 candidates in APOGEE and SDSS DR9, respectively. From these figures we can see, APOGEE candidates are near the tip of the red giant branch, most near the Pal 5 core; SDSS candidates are red giants and RR Lyraes. These SDSS red giants are far from the center while RR Lyraes are near the Pal 5 cluster center. Metallicities

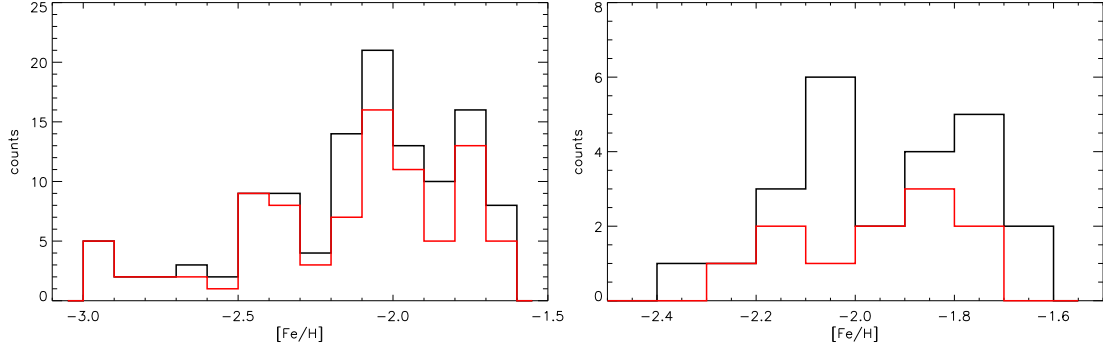


Fig. 8 The left panel and the right panel are the metallicity distributions of Orphan stream candidates in SDSS and LAMOST data respectively. In each panel, the red histogram is the metallicity distribution of stars within $T_{Orphan} \pm 17.5 \text{ km s}^{-1}$, while the black histogram is for stars within $T_{Orphan} \pm 35 \text{ km s}^{-1}$.

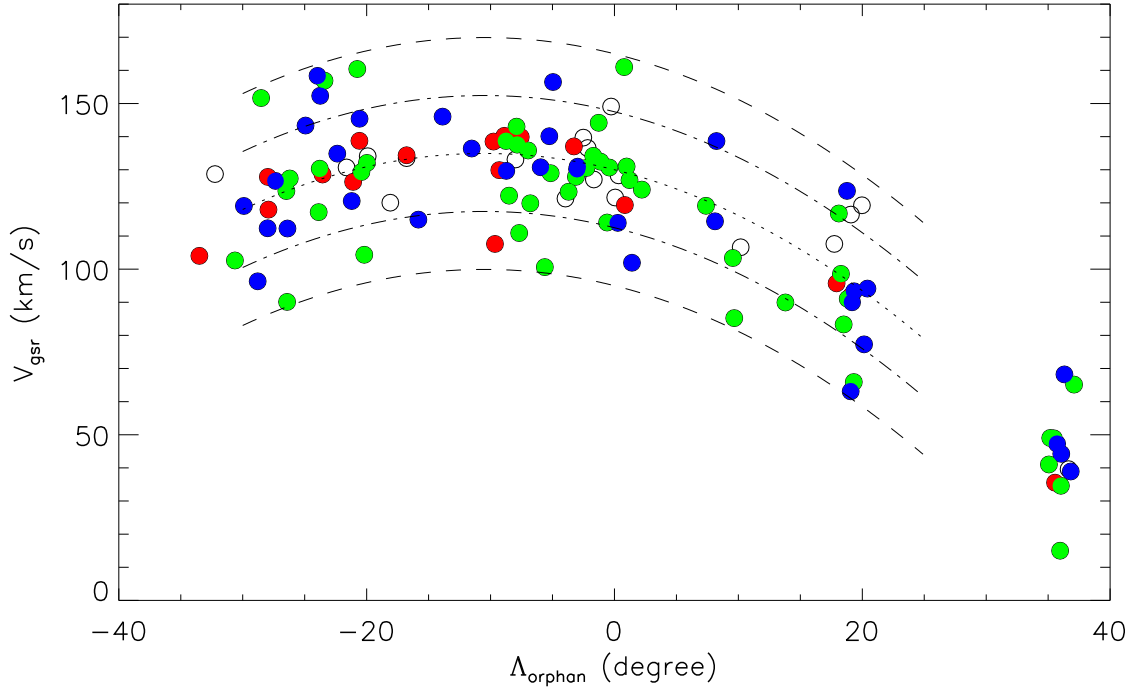


Fig. 9 This figure shows the V_{gsr} of SDSS candidates along the Λ_{Orphan} . The dash dot lines are $T_{Orphan} \pm 17.5 \text{ km s}^{-1}$, while the dash lines are $T_{Orphan} \pm 35 \text{ km s}^{-1}$. The central dot line is $T_{Orphan} \text{ km s}^{-1}$. All candidates are marked by circles, while stars with $[\text{Fe}/\text{H}]$ in $[-2.5, -2.3]$, $[-2.2, -1.9]$, and $[-1.9, -1.6]$ are marked by red, green and blue circles, respectively.

-1.41 given by the Harris catalogue. SDSS candidates metallicity should be within $[-1.9, -1.4]$, as shown in the left panel of Fig. 12, which is lower than those given by APOGEE, Kuzma et al. (2015) and the Harris catalogue. For the line-of-sight velocity, its distribution of APOGEE candidates is very narrow which con-

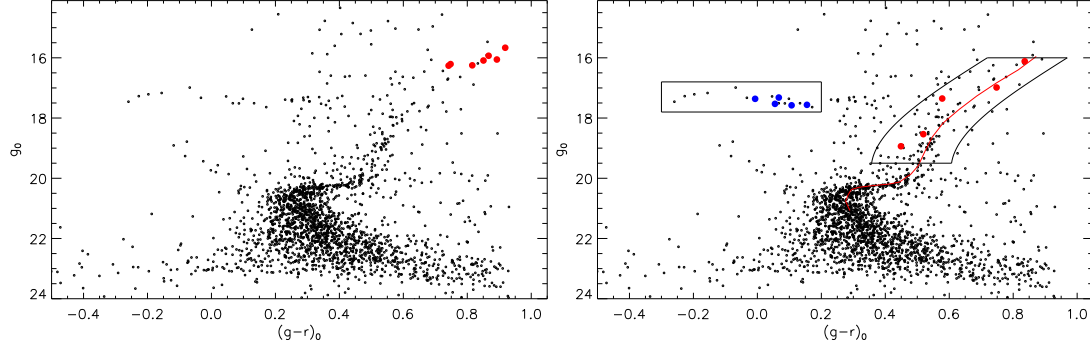


Fig. 10 Left panel: the CMD of APOGEE candidates in the Pal5 tidal stream; Right panel: the CMD of SDSS candidates in the Pal5 tidal stream. In each panel, the background stars are within $8.3'$ around Pal 5 cluster center. Red circles are red giants, while blue circles are RR Lyraes. In the right panel, areas enclosed by black lines are where we select candidates in SDSS DR9, while the red line is the fiducial sequence of Pal 5 given by An et al. (2008).

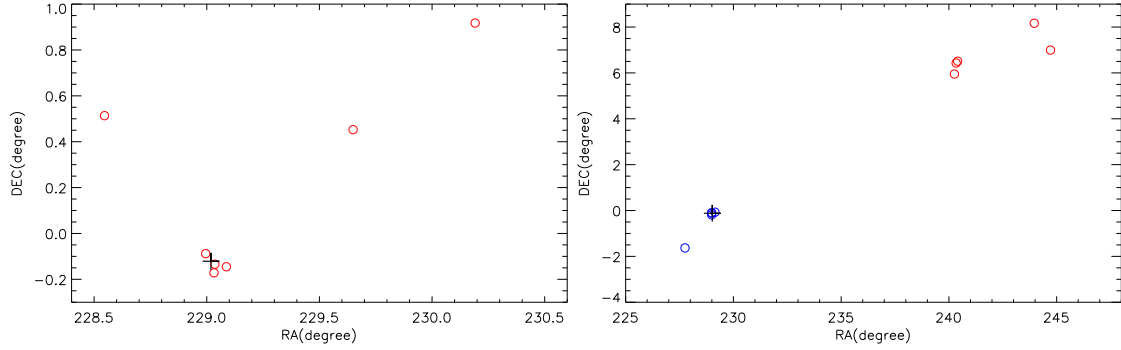


Fig. 11 Left panel: APOGEE candidate positions; Right panel: SDSS candidate positions. Red circles are red giants, while blue circles are RR Lyraes. Black cross is Pal 5 cluster center in each panel.

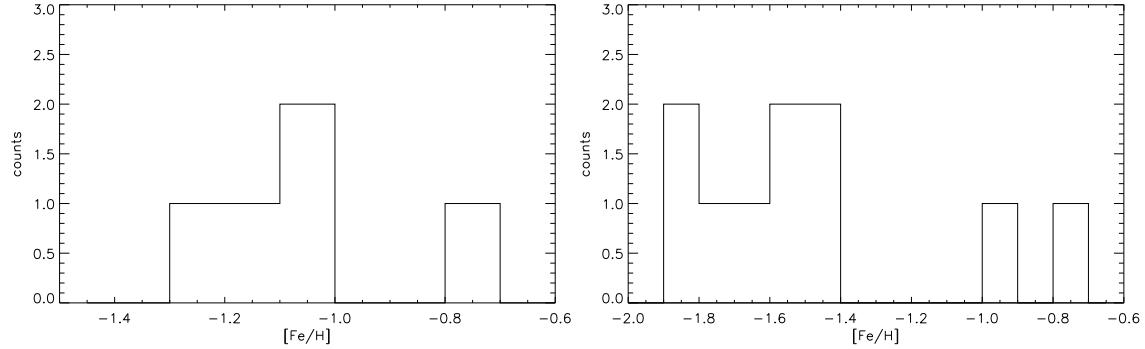


Fig. 12 Left panel: Metallicity distribution of Pal 5 candidates in APOGEE; Right panel: Metallicity distribution of Pal 5 candidates in SDSS DR9.

As the APOGEE candidates and SDSS RR Lyraes are all in the Pal 5 cluster, so they are bona fide members, then their confidence levels are set to 1. The 5 SDSS red giants are all far from Pal 5 center, so their confidence levels are set to 2.

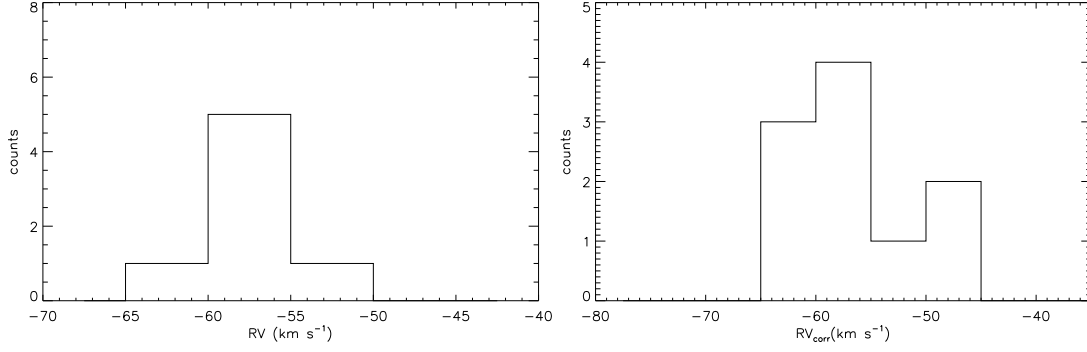


Fig. 13 Left panel: Line of sight velocity distribution of APOGEE candidates. Because APOGEE candidates all are around Pal 5 cluster center, corrected velocity is not used. Right panel: Corrected velocity distribution of SDSS candidates.

3 CONCLUSION AND DISCUSSION

In this paper, we present 3 tables of high confidence candidate stellar members of the GD-1, CPS, Orphan and Pal 5 tidal streams from LAMOST DR3, SDSS DR9 and APOGEE spectroscopic catalogs. In LAMOST DR3, we find 20, 4, 24 high confidence candidates of the GD-1 stream, CPS and the Orphan stream, respectively. In SDSS DR9, we find 59, 118, 10 high confidence candidates of CPS, Orphan stream and Pal 5 tidal stream, respectively. In APOGEE, we find 7 Pal 5 high confidence candidates. Table 1 lists the LAMOST DR3 candidates, including ID, position, spectral type, and radial velocity, $[\text{Fe}/\text{H}]$, $\log g$, T_{eff} with their errors. Table 2 lists the SDSS data, including plate, mjd, fiberid, position, spectral type, and radial velocity, $[\text{Fe}/\text{H}]$, FEHWBG, $\log g$, T_{eff} with their errors. Table 3 gives the information for each APOGEE candidate, including ID, position, and radial velocity, T_{eff} , $[\text{Fe}/\text{H}]$, $\log g$ with their errors. The last column in these 3 tables show the confidence level (described by 1, 2, 3) of each candidates, with a higher number indicating lower confidence.

Of note: (1) The brightest stars of GD-1 and Orphan streams, are all from LAMOST data, so the LAMOST data supplements the bright end of these streams.

(2) LAMOST and SDSS Orphan stream data show that there may be 2 or 3 metallicity peaks, and the most metal-poor peak rests at $\Lambda_{\text{Orphan}} < 0$. Alternatively, there may be stars from other streams or coherent background or foreground halo structures in this direction on the sky. The Orphan stream may span a broader area for regions beyond $\Lambda_{\text{Orphan}} < -20^\circ$ and $\Lambda_{\text{Orphan}} > 10^\circ$.

(3) The cataloged APOGEE metallicity for Pal 5 is around -1.2 which is significantly higher than that given by the globular cluster and SDSS literature which quote $[\text{Fe}/\text{H}] \sim -1.4$. APOGEE spectra are obtained with a high resolution infrared spectrograph and measure elements besides Iron or Magnesium or Calcium to determine metallicity.

In the future, we plan to continue to probe the abundances of stream stars, including searches for gradients in abundance along the streams, in order to better understand the streams' formation and evolution histories.

Finally, we hope to use these additional candidate stream stars' velocity, metallicity and membership

potential can then be used to constrain the potential significantly better than fitting any single stream by itself and help resolve remaining questions about the extent and shape of our dark matter halo Newberg et al. (2010); Willett et al. (2009); Law, Majewski and Johnston (2009).

Acknowledgements This research is supported by the Natural Science Foundation of China for the Youth under grants Y011161001, National Science Foundation of China (NSFC) under grant No. 11403056, the National Natural Science Foundation of China (11673036) and NSFC Key Program NSFC-11333004. Support was provided by the US NSF LAMOST-PLUS grant. Y. Wu acknowledges the fund supplied by the Guangdong Provincial Engineering Technology Research Center for Data Science. We also thank the referee for valuable advice.

Guoshoujing Telescope (the Large Sky Area Multi-Object Fiber Spectroscopic Telescope LAMOST) is a National Major Scientific Project built by the Chinese Academy of Sciences. Funding for the project has been provided by the National Development and Reform Commission. LAMOST is operated and managed by the National Astronomical Observatories, Chinese Academy of Sciences.

References

- Alam S. et al., 2015, *ApJS*, 219, 12
 An, D., et al., 2008, *ApJS*, 179, 326
 Belokurov, V., et al., 2006, *ApJ*, 642, L137
 Carlberg R. G., Grillmair C. J., Hetherington N., 2012, *ApJ*, 760, 75
 Cui X. Q., et al., 2012, *RAA*, 12, 1197
 Eggen, O. J., Lynden-Bell, D., & Sandage, A. R. 1962, *ApJ*, 136, 748
 Gao, H., et al., 2015, *RAA*, 15, 2204
 Grillmair, C. J., & Dionatos, O., 2006, *ApJ*, 643, L17
 Kuzma, P. B., et al., 2015, *MNRAS*, 446, 3297
 Law, DR, Majewski SR, & Johnston KV, 2009 *ApJ* 703, L67
 Luo A L., et al., 2012, *RAA*, 12, 1243
 Ibata, R., Gilmore, G., Irwin, M. J., 1994, *Nature*, 370, 194
 Ibata, R. A., et al., 2003, *MNRAS*, 340, 21
 Majewski, S. R., et al., 2003, *ApJ*, 599, 1082
 Majewski, S. R., et al., 2015, *arXiv:1509.05420*
 Newberg, H. J., et al., 2009, *ApJ*, 700, 61
 Newberg, H. J., et al., 2010, *ApJ*, 711, 32
 Odenkirchen M., et al., 2001, *ApJ*, 548, L165
 Odenkirchen, M., et al., 2003, *AJ*, 126, 2385
 Schlafly, E.F. & Finkbeiner, D.P., 2011, *ApJ*, 737, 103
 Schlegel, D. J., Finkbeiner, D. P., & Davis, M. 1998, *ApJ*, 500, 525
 Searle, L., & Zinn, R. 1978, *ApJ*, 225, 357
 Su D. & Cui X. Q., 2004, *Chinese Journal of Astronomy and Astrophysics*, 4, 1

- Wilhelm, R., et al., 1999, AJ, 117, 2308
- Willett, B. A., et al., 2009, ApJ, 697, 207
- Wu, Y., et al., 2014, IAUS, Volume 10, Issue S306, pp. 340-342
- Yanny, B., et al., 2003, ApJ, 588, 824
- Yanny, B., et al., 2009, ApJ, 700, 1282Y
- Yanny, B., et al. 2009, AJ, 137, 4377Y
- Yam, W., et al., 2013, ApJ, 776, 133
- York, D. G., et al., 2000, AJ, 120, 1579
- Zhao G., et al., 2012, RAA, 12, 723

Table 1 Candidates in LAMOST

stream	obsid ^a	subclass	ra (deg)	dec (deg)	rv^b (km s ⁻¹)	T_{eff} (K)	[Fe/H]	logg	rv_{err} (km s ⁻¹)	$T_{\text{eff-err}}$ (K)	[Fe/H] _{err}	logg_err	level ^b
GD1	196716136	G5	125.22538757	-2.78869820	253.37	5001.74	-1.78	2.32	29.10	186.84	0.29	1.08	3
GD1	187405120	G7	137.72410583	21.93488503	135.74	4459.66	-1.55	1.41	48.83	344.33	0.61	1.21	3
GD1	132513055	G0	139.29585266	23.10439491	119.02	5212.79	-1.86	2.86	42.48	211.86	0.37	1.16	3
GD1	313108245	K3	125.95130157	-1.41831505	261.85	4246.94	-1.74	0.55	17.33	64.31	0.09	0.29	3
GD1	343405145	G3	155.50750732	41.43789673	-75.93	4489.56	-1.98	0.88	20.57	61.48	0.10	0.37	1
GD1	136814012	F2	153.97523499	40.22281265	-29.44	5034.87	-2.21	2.36	48.94	266.52	0.47	1.21	2
GD1	31709120	G3	153.46257019	41.59279633	-84.04	4815.06	-1.64	1.86	25.35	250.98	0.41	1.10	2
GD1	19114174	G0	143.17625427	28.68422318	33.63	4878.86	-2.24	1.86	47.26	216.92	0.36	1.08	1
...												

^a Observation ID: the same object in different observation has different obsid which is unique for all LAMOST spectra.

^b Heliocentric heliocentric velocity.

^c The confidence level: 1 represents highest confidence.

Note: Only a portion of Table is shown here for illustration. The whole Table contains information of 48 stream candidates in LAMOST is available in the online electronic version.

Table 2 Candidates in SDSS

stream	plate	mjd	fiberid	subclass	ra	dec	rv^a	T_{eff}	[Fe/H]	FEHWBG	logg	rv_{err}	$T_{\text{eff_err}}$	[Fe/H]_err	FEHWBG_err	logg_err	level ^b
					(deg)	(deg)	(km s ⁻¹)	(K)				(km s ⁻¹)	(K)				
Cetus	2864	54467	91	F9	18.992146	-10.615119	-61.74	4868.47	-2.16		1.62	1.62	55.22	0.06		0.14	1
Cetus	2878	54465	59	A0p	22.955864	-10.540712	-51.03	8456.75	-2.10	-2.10	3.39	7.31	141.34	0.29	0.29	0.29	1
Cetus	2864	54467	49	A0	19.162479	-10.344024	-54.14	7878.93	-1.72	-2.46	3.03	4.75	102.53	0.06	0.14	0.27	1
Cetus	3109	54833	111	F9	16.801901	-10.321400	-60.38	4473.98	-2.28		1.26	1.53	151.87	0.03		0.13	1
Cetus	2864	54467	102	G2	19.334705	-10.221816	-68.46	5151.40	-2.13		1.97	3.39	45.32	0.03		0.11	1
Cetus	2865	54503	269	G2	24.394780	-9.886655	-65.46	5153.11	-2.40		2.24	3.58	59.23	0.05		0.22	1
Cetus	2878	54465	312	A0p	20.752808	-9.660568	-73.00	8294.23	-1.92	-2.42	3.25	8.20	144.40	0.16	0.28	0.07	1
Cetus	2864	54467	351	F9	17.415293	-9.638273	-70.09	4912.60	-2.25		1.48	2.09	9.19	0.05		0.12	1
...																

^a Heliocentric heliocentric velocity.

^b The confidence level: the lower number the higher confidence.

Note: Only a portion of Table is shown here for illustration. The whole Table contains information of 187 stream candidates in SDSS is available in the online electronic version.

Candidates of streams

Table 3 Candidates in APOGEE

stream	ID	ra (deg)	dec (deg)	rv^a (km s ⁻¹)	T_{eff} (K)	[Fe/H] .	logg	rv_{err} (km s ⁻¹)	$T_{\text{eff_err}}$ (K)	[Fe/H]_err	logg_err	level ^b
Pal5	2M15160773-0010183	229.032225	-0.171773	-58.11	5119.35	-0.79	1.98	0.38	91.47	0.05	0.11	1
Pal5	2M15162090-0008426	229.087113	-0.145193	-57.70	4408.65	-1.09	1.12	0.16	91.47	0.05	0.11	1
Pal5	2M15160866-0008031	229.036088	-0.134211	-64.40				0.30				1
Pal5	2M15155888-0005171	228.995349	-0.088101	-56.77	4400.08	-1.25	0.87	0.12	91.47	0.05	0.11	1
Pal5	2M15183589+0027100	229.649545	0.452789	-57.41	4584.16	-1.07	1.94	0.10	91.47	0.05	0.11	1
Pal5	2M15141111+0030487	228.546300	0.513550	-54.43				4.27				1
Pal5	2M15204588+0055032	230.191207	0.917572	-56.09	4494.36	-1.18	1.27	0.09	91.47	0.05	0.11	1

^a Heliocentric heliocentric velocity.^b The confidence level: 1 indicates highest confidence.